Volume 16, Issue 3, 162518 (1-13)

International Journal of Nano Dimension (IJND)

https://dx.doi.org/10.57647/j.ijnd.2025.1603.18

Energy transition in bioconvective darcy-forchheimer nanofluid flow: A numerical study

Najmeh Hajialigol*

Mechanical Engineering Department, Hamedan University of Technology, Hamedan, Iran.

***Corresponding author:** n.hajialigol@hut.ac.ir

Original Research

Received:
28 March 2024
Revised:
8 December 2024
Accepted:
14 December 2024
Published online:
1 June 2025

Abstract:

Darcy-Forchheimer nanofluids (NF) can be utilized to develop oil recovery efficiency from oil reservoirs. Nanoparticles in the NF can aid in increasing rock permeability, reducing oil viscosity, and facilitating oil flow to wells. Unsteady Darcy-Forschheimer NF bioconvective flow with activation energy and Arrhenius chemical reaction on a permeable tensile surface was investigated. The flow equations are partial differential equations that are translated into ordinary differential equations (ODE) using suitable similarity transformations. Runge–Kutta integration with the shooting method of modified Newton–Raphson methods was used to resolve these ODEs numerically. Several graphs and tables were utilized to display how changes in the evolving parameters influence the flow fields. The result demonstrated that the unsteadiness parameter, porous medium permeability, Hartmann number, porosity parameter, and Grashof parameter increased the velocity profile, while the buoyancy ratio decreased it. Unsteadiness parameter, Hartmann number, buoyancy ratio, bioconvective Rayleigh number, Prandtl number, Eckert number, and internal heat generation raised the temperature profile. The porosity parameter, Grashof number, and radiation parameter led to a decrease in temperature profile. The unsteadiness parameter, Hartmann number, buoyancy ratio, thermophoresis, Prandtl number, and Eckert number reduced the concentration profile. The growth of the parameter of internal heat generation had almost no effect on the concentration profile. The radiation parameter and Brownian motion enhanced the concentration profile.

Keywords: Activation energy; Darcy-Forchheimer; Magnetohydrodynamics; Nanofluid; Porous medium

1. Introduction

Bioconvection, a fascinating phenomenon in fluid mechanics, involves organized and spontaneous microorganism movements such as algae or bacteria in response to environmental stimuli. This phenomenon is highlighted because of the exciting and complex patterns it generates in the liquid medium. This phenomenon is highlighted due to the complexity and intriguing patterns it creates in fluid media. The basic principles governing microbial interactions and a wide range of applications in different fields are discovered by addressing the bioconvection complexities. Bioconvection originates from the microorganism's collective behavior that responds to environmental cues such as nutrient distribution, temperature gradient, or light [1]. The presence of interactions between these microorganisms results in the appearance of organized fluid movement configurations that create complex and remarkable visual structures. Bioconvection in natural aquatic environments plays a central role in nutrient mixing, affects organism distribution, and contributes to the ecosystem dynamics.

Bioconvection is used in different biotechnological processes. Organized movement of microorganisms in bioreactors leads to increased mass transfer and improved process efficiency, including wastewater treatment and fermentation [2], which has consequences for economic and practical bioprocessing. Considering the microorganism behavior in response to particular conditions has possible applications in medicine. This awareness can help develop diagnostic tools or target drug delivery systems [3]. Various patterns of bioconvection can act as environmental health indicators. Any alteration in microbial behavior manifests itself in the dynamics of bioconvection and can serve as primary warning signals for ecological pollution or disturbance, helping efforts to monitor the environment [4]. The bioconvection is currently being investigated by researchers for its possible application in lab-on-a-chip technologies and microfluidic apparatus. The functionality of microorganisms for controlled movement of fluid promises advances in point-of-care and diagnostic uses [5]. The bioconvection process

has consequences for the production of renewable energy. Using the microorganism self-organization can improve processes such as the production of microbial fuel cells or biofuel and help to viable energy solutions [6].

The understanding obtained from the study of bioconvection can motivate bio-inspired material development with unique flow characteristics. Instead, the model of Darcy-Forchheimer considers that nanoparticles at higher concentrations result in cluster formation that behaves differently than separate nanoparticles due to interactions with each other. This model forecasts that with increasing nanoparticle concentration, the nanofluid (NF) thermal conductivity should increase nonlinearly, although the viscosity must be enhanced more than the Williamson model [7]. NFs are known as nanoparticle colloidal suspensions in a base fluid, which have attracted attention due to their distinct flow and thermal properties. The Darcy-Forchheimer NF applications, which consider the further resistor to flow in a porous medium, offer encouraging ways in numerous scopes. It should be noted that the thermal conductivity is enhanced by nanoparticle inclusion in fluid [8].

Shafiq et al. [9] investigated the incremental effect of thermal radiation on heat transfer improvement corresponding to the Darcy–Forchheimer flow of carbon nanotubes along a stretched rotating surface using RSM. For this purpose, they studied Casson carbon nanotubes' constructed model in boundary layer flow by implications of both single-walled CNTs and multi-walled CNTs. They utilized the Runge–Kutta Fehlberg technique of shooting to numerically solve transformed nonlinear ordinary differential systems. Their results showed that the sensitivity of SFC via SWCNT-Water became higher by increasing values of permeability number. Also, the sensitivity of SFC via SWCNT-water towards the permeability number was higher than the solid volume fraction for medium and higher permeability levels. In another study, Shafiq et al. [10] utilized the Levenberg-Marquardt method with backpropagated neural networks to evaluate the nanomaterial flow of the Darcy-Forchheimer Sisko fluid model. They considered thermophoresis and Brownian motion effects when developing the nanofluid model. They stated that the original nonlinear coupled partial differential system representing the fluidic model was converted to an analogous nonlinear ordinary differential system. A dataset for the proposed multilayer perceptron artificial neural network was produced by altering the necessary variables via the Galerkin weighted residual approach for different fluid model scenarios. It should be noted that artificial neural networks have been used for the modeling of Darcy Forchheimer NFs in different fields, which has also had interesting results [11–17].

The effect of thermal radiation and bioconvection on MHD Williamson Casson NF flow with the Gyrotactic microorganism swimming due to a porous tensile plate was studied by Jawad et al. [18]. It was found that the microorganism field decreases with the increasing bioconvection value and Peclet number. Mass flux and fluid are directed toward a porous tensile plate. It can be seen that the physical interpretation of thermo-physical parameters is ascending in density, energy, and highly concentrated fields. The Brownian motion, non-Newtonian Williamson parameter, Peclet number, bio-convection, mixed convection Hartman number, mixed convection, Casson parameter, bioconvection Rayleigh number, and thermophoresis diffusion terms are among the many prominent terms for which the valuations are graphically achieved. Sharma and Gandhi [19] discussed the combined impacts of nonuniform heat sink/source and Joule heating on unsteady MHD mixed convective flow on a vertical tensile surface embedded in a Darcy-Forchheimer porous media. A constant transverse magnetic field was applied on the porous surface. Additionally, the influences of sliding velocity, temperature, and concentration were examined. A set of ODEs was created from the coupled NL partial differential equations governing the system through the use of similarity transformation. Presenting real-world applications in engineering and industrial operations through various graphs is the flow feature physical representation that arose in this problem.

Shafiq et al. [20] studied the gradual influence of nonlinear thermal radiation on the improvement of heat transfer related to the flow of nanofluids over a stretched rotating surface by the Darcy–Forchheimer law. They analyzed the data from the local skin friction coefficient (LSFC) and local Nusselt number (LNN) using various statistical distributions, and it was determined that both datasets generally fit the exponentiated Weibull distribution for various values of considered parameters. In another study, Shafiq et al. [21] implemented a sensitivity analysis using response surface strategies to control the Walters-B nanofluid stagnant point flow caused by a Riga surface. They utilized the Buongiorno model to construct the mathematical model, which includes a Newtonian heating condition as well as radiation effects. Their outcomes showed that the sensitivity of LNN to the Brownian number decreases with the growing thermophoresis number but the sensitivity value also varies from positive to negative for all values of the Brownian number.

Tadesse et al. [22] examined the hydromagnetic stagnation point of a magnetic ferrofluid next to a permeable convectively heated shrinking/tensile plate in a Darcy-Forchheimer porous media. They found that the upper branch solution is physically feasible, and hydrodynamically stable, although the lower branch solution is physically impractical and unstable. Suction/injection, magnetic field parameter and volume fraction of magnetite nanoparticles are augmented to maintain fluid flow stability. Conversely, the flow stability is inflated by the porous medium inertia and porous medium parameters. Vedavath et al. [23] numerically investigate the radiative non-Darcy NF flow on a tensile plate with conditions of convective Nield and energy activation. Their results were obtained by examining the graphical influence of different thermophysical parameters on the nanoparticle volume fraction, momentum, and energy distributions. With the increase in temperature, it can be seen that the rise in Darcy's number causes a decrease in fluid velocity and nanoparticle concentration. Increasing the Forchheimer number and velocity slip parameter leads to similar behavior. Shafiq et al. [24] analyzed the combined effects of activation energy with a binary chemical reactant in a

steady magnetohydrodynamic mixed convective third-grade nanofluid flow by radially radiative stretching plate with an artificial intelligence approach. They found that the initial nonlinear coupled partial differential equations expressing the fluid model were formed as a comparable nonlinear ordinary differential equations system by incorporating appropriate transformations. The obtained results showed that artificial neural networks are an engineering tool that can be used with high accuracy to estimate the combined effects of activation energy and binary chemical reaction in a fixed magnetohydrodynamic mixed convective third-grade nanofluid flow with a radial radiative stretched plate.

Zhang et al. [25] investigated the nonlinear NF flow under the effects of Arrhenius kinetics and Lorentz forces via a porous surface. They evaluated the impact of the Brownian motion, porous media, magnetic, Arrhenius function, radiation, and thermophoresis factors on the velocity, distribution of nanoparticles (concentrations), and temperature. They found that the concentration values of nanoparticles are significantly increased by increasing the activation energy parameter values. The concentration of nanoparticles and the temperature rise with increasing the thermophoresis parameter. The thickness of the thermal boundary layer (TBL) and temperature are enhanced with growth in radiation parameters. Both the Brownian motion parameter and Schmidt number are rising (smaller nanoparticles). Since NFs show significant heat transfer capabilities compared to pure fluids in various engineering and industrial uses, the dynamic study of NFs with bioconvection impacts has essential uses. Considering such outstanding potentials, Khan et al. [26] investigated the effect of bioconvective micropolar NF flow on a moving thin needle comprising gyrostatic microorganisms. They converted the governing equations into a dimensionless form using a set of appropriate variables, and then the homotopy analysis method (HAM) was used to resolve them. The primary outcomes of this work demonstrate that an increase in the buoyancy ratio parameter causes the micropolar fluid to be redirected towards the surface of the needle. As a result, the fluid flow decreases. Enhancing Eckert's number is related to increasing the energy used for transportation, which raises the temperature. Shafiq et al. [27] investigated the constructed model of a tangent hyperbolic nanofluid in boundary layer flow with implications of thermophoresis and Brownian motion. They discovered that the sensitivity of the local Nusselt number increments by expanding Lewis and thermophoresis numbers while the highest non-dimensional Nusselt number appears close to the significant level for the thermophoresis and low level for the Brownian motion variable. Furthermore, it was shown that the average maximum mean thickness of motile microorganisms appears at the highest level of Brownian motion and thermophoresis number and thermophoresis and Lewis numbers.

Bhatti et al. [28] investigated the higher-order Darcy-Forchheimer Eyring-Powell NF slip flow with bioconvection and NL thermal radiation occurrence. Their results illustrated that the velocity of the fluid is controlled using inertial impact magnetic force. Although the slip parameter had a decreasing trend, the velocity was improved with the Eyring-Powell fluid parameter. Habib et al. [29] evaluated the influences of activation energy, double diffusion and bioconvection on the Maxwell, Williamson and micropolar NFs flows due to a tensile surface. They concluded that Newtonian, Williamson and Darcy fluids followed by micropolar fluids have the lowest velocity values. Raham et al. [30] studied activation energy and mixed convection influences on MHD bioconvective NF flow by assessing irreversibility. They reported that the velocity profile decreases with increased magnetic parameters and Darcy-Forchheimer number. Also, they found that the Bejan number decreases with increasing Brinkman variables, while entropy generation increases for higher Brinkman variables. Recently, Jawad et al. [31] analyzed the MHD Darcy-Forchheimer flow of Casson nanofluid as having a rotating disk with Arrhenius activation energy and thermal radiation. Their findings demonstrated that increasing the Reynolds number decreased the tangential NF velocity. Also, the tangential and radial velocities decreased with increasing the magnetic factor. Tamilzharasan et al. [32] studied the convection of magneto-mixed Williamson NF flow via a double-stratified porous media in activation energy presence. They found that the nanofluid temperature and concentration reduced with the more significant thermal and mass stratification parameters estimation.

Thermal radiation impacts of the flow of Darcy-Forchheimer Maxwell fluid along a tensile surface with exponential activated energy were investigated by Rashid et al. [33]. Also, the influence of thermal radiation, chemical reactions, and convective boundary conditions on the 3D Darcy-Forchheimer NF flow on a rotating surface with Arrhenius-activated energy was studied by Shafiq et al. [34]. Hayat et al. [35] evaluated binary chemical reaction, activation energy, and entropy formation influences on the Williamson NF Darcy-Forchheimer flow via a smooth NL stretchable surface. It should be noted that the activation energy is the minimum energy amount required in a system to create a chemical reaction. There are two kinds of energy: potential and kinetic. The reaction between molecules may be due to the loss of insufficient collisions or kinetic energy. Only a minimal amount of energy is needed to start a chemical reaction at this stage. The activation energy effect on the expected behavior in a permeable boundary layer was first investigated by Bestman [36]. NL tensile plates in the activated-energy pseudo-plastic magnetohydrodynamic NF flow were studied by Dawar et al. [37]. The result displays that the profile of velocity decreases with the Forschheimer and Weissenberg numbers, although the mixed convection parameter illustrates a tendency to increase the profile of velocity. Alsaadi et al. [38] evaluated the homotopy analysis method to investigate the energy equation of Arrhenius in magneto-Williamson NF flow. The result displays that the distribution of temperature increases with mass relaxation time, irradiance amounts to higher estimates of high thermal relaxation time and Schmidt number, while the concentration profile decreases. Increasing the parameters of mass, and thermal stratification causes a decrease in temperature. Muhammad et al. [39] investigated the impact of the entropy approach, porosity, slip and activation energy parameter on

the mixed convective flow of Darcy–Forchheimer along a stretched curved surface.

Mixed convective heat transfer in a turbulent NF flow was studied by Danook et al. [40]. The unsteady flow of a solar irradiated non-Newtonian Casson NF was investigated by Jamshed et al. [41] through the Keller box method. Alghamdi et al. [42] studied the effect of MHD mixed convective Casson NF flows on a tensile irregular surface vertically submerged in a porous Darcy-Brinkman media. Arain et al. [43] analyzed Arrhenius kinetics between rotating circular plates in multiphase flow. Their research indicates that since the shear-thinning fluid has a higher velocity than the Newtonian and shear-thickening cases, the fluid viscosity decreases with shear strain. The axial velocity distribution is affected by the Carreau fluid velocity in the Newtonian case ($n = 0$), shear-thinning ($n < 1$), and shear-thickening ($n > 1$) scenarios.

2. Materials and methods

The present study deals with the gyrostatic boundary layer microorganisms driving the flow of a water-based NF in the vertical permeable plate as shown in Fig. 1, a constant transverse uniform free stream velocity $u = U_0(x)$ is used for the flow. Since the voltage is low and there is no magnetic field, magnetic Reynolds number and Hall impacts are negligible. As stated, it is predicted that the nanoparticles will not influence the speed or direction of microorganism movement. The dispersion of nanoparticles is believed to be unstable (no coagulation of nanoparticles) and dilute (no particle concentration greater than 1%). This hypothesis is reasonable because NF bioconvection is anticipated to occur only in a diluted nanomaterial suspension. In the absence of this, the high nanomaterial concentration prevents bioconvection and enhances the viscosity of the base fluid. The framework of bioconvection induced by oxytactic microbes is based on the Algehyne et al. [44] methodology.

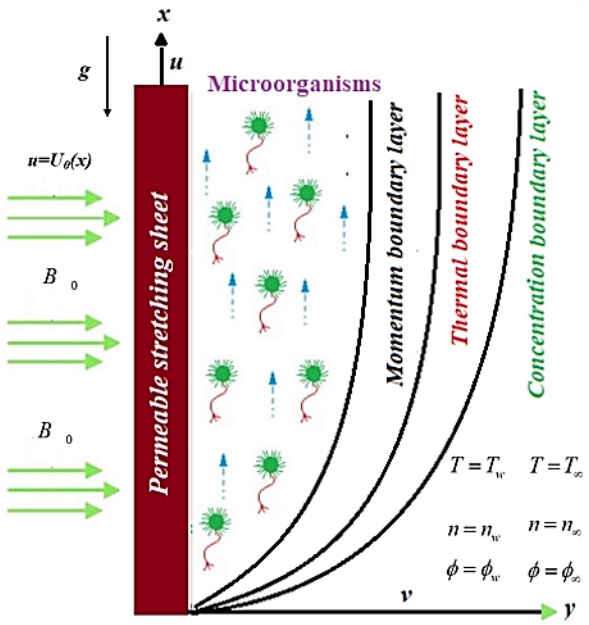

Figure 1. Fluid flow via the vertical permeable plate [44].

2.1 Model development

The work performed was developed. Therefore, the new model is as follows [44]:

Equation of continuity and momentum:

$$\frac{\partial u}{\partial x}+\frac{\partial v}{\partial y}=0 \tag{1}$$

$$\begin{aligned}\frac{\partial u}{\partial t}+u\frac{\partial u}{\partial x}+v\frac{\partial u}{\partial y}&=u_\infty\frac{\partial u_\infty}{\partial x}+\nu_f\frac{\partial^2 u}{\partial y^2}\\&+\frac{1}{P_f}\left[(1-C_\infty)P_f(T-T_\infty)\beta_g-(\rho_p-\rho_f)(C-C_\infty)g\right.\\&\left.-(n-n_\infty)(\rho_m-\rho_f)g\gamma\right]-\frac{\nu}{k}(u-u_\infty)\\&-\frac{k'}{\sqrt{k}}(u^2-U_\infty^2)-\frac{\sigma B_0^2}{\rho_f}(u-U_\infty)\end{aligned} \tag{2}$$

Energy equation:

$$\begin{aligned}\frac{\partial T}{\partial t}+u\frac{\partial T}{\partial x}+v\frac{\partial T}{\partial y}&=\alpha\left(\frac{\partial^2 T}{\partial x^2}+\frac{\partial^2 T}{\partial y^2}\right)+\lambda\left[D_b\frac{\partial C}{\partial y}\frac{\partial T}{\partial y}\right.\\&\left.+\left(\frac{D_T}{T_\infty}\right)\left(\left(\frac{\partial T}{\partial x}\right)^2+\left(\frac{\partial T}{\partial y}\right)^2\right)\right]+\frac{\mu\alpha}{k}\left(\frac{\partial u}{\partial t}\right)^2\\&+\alpha\frac{\sigma B_0^2}{k}\mu^2+\frac{Q_0}{(\rho c)_f}(T-T_\infty)-\frac{1}{(\rho c)_f}\frac{\partial q_r}{\partial y}\\&+\frac{D_m k_r}{c_s c_p}\frac{\partial^2 C}{\partial y^2}\end{aligned} \tag{3}$$

Concentration equation:

$$\begin{aligned}\frac{\partial C}{\partial t}+u\frac{\partial C}{\partial x}+v\frac{\partial C}{\partial y}&=D_B\left(\frac{\partial^2 C}{\partial y^2}\right)+\left(\frac{D_T}{T_\infty}\right)\left(\frac{\partial^2 T}{\partial x^2}+\frac{\partial^2 T}{\partial y^2}\right)\\&-k_r^2\left(\frac{T}{T_\infty}\right)^n(C-C_\infty)\exp\left(-\frac{E_a}{kT}\right)+\frac{D_T}{T_\infty}\frac{\partial^2 T}{\partial y^2}\end{aligned} \tag{4}$$

$$\begin{aligned}\frac{\partial n}{\partial t}+u\frac{\partial n}{\partial x}+v\frac{\partial n}{\partial y}+\frac{bW_c}{C_w-C_\infty}\left(\frac{\partial}{\partial y}\left(n\frac{\partial c}{\partial y}\right)+\frac{\partial}{\partial x}\left(n\frac{\partial c}{\partial x}\right)\right)\\=D_m\left(\frac{\partial^2 n}{\partial x^2}+\frac{\partial^2 n}{\partial y^2}+2\frac{\partial^2 n}{\partial y\partial x}\right)\end{aligned} \tag{5}$$

Here (u, v) determine the velocity component, ρ_f is the density, Q_0 is the heat source, U_∞ is the uniform free stream velocity, α is the thermal diffusivity, $k = k_0 x$ is the Darcy permeability of the permeable medium, $k' = \frac{k_0}{\sqrt{x}}$ is the Forchhemier resistance, k_0 is the initial permeability, D_m is the microorganism diffusivity, g and β are the gravity and volume expansion, respectively, σ is the electrical conductivity, μ is the viscosity, $\lambda = (\rho C)_p/(\rho C)_f$ is the ratio of the heat capacitance to the base fluid, γ is the microorganism average volume, W_c is cell moving speed, b is the chemotaxis coefficient, n is the concentration of the microorganisms and ρ_m represent their density.

The corresponding boundary conditions are given by Eq. (6):

$$\begin{cases} u = U_\infty(x),\ v = V,\ T = T_w,\ \varphi = \varphi_w,\ n = n_w & \text{at } y = 0\\ u = 0,\ v = 0,\ T \to T_\infty,\ \varphi = \varphi_\infty,\ n \to n_\infty & \text{as } y \to \infty\end{cases} \tag{6}$$

where n_w, φ_w, and T_w are the density of motile microbes, volume fraction of nanoparticles and surface temperature. Similarly, the ambient values are signified as n_∞ , φ_∞ , and T_∞ respectively.
With the similarities variables as below (Eq. 7):

$$\begin{aligned}&\eta = y\sqrt{\frac{a}{\nu}},\ \psi = \sqrt{a\nu}xf,\ u = \frac{\partial\psi}{\partial y},\ v = -\frac{\partial\psi}{\partial x},\\ &\theta = \frac{T-T_\infty}{T_w-T_\infty},\ \varphi = \frac{C-C_\infty}{C_w-C_\infty},\ X = \frac{n-n_\infty}{n_w-n_\infty},\\ &T = \theta(T_w-T_\infty)+T_m,\ C = \varphi(C_w-C_\infty)+C_\infty\end{aligned} \tag{7}$$

We get

$$\begin{aligned}&f'''+(f-\frac{c_1\eta}{2a})f''-(f')^2-f_n((f')^2-1)\\ &\quad -Ha(f'-1)+Gr(\theta-Nr\varphi-R_bX_1)=0\end{aligned} \tag{8}$$

$$\begin{aligned}&\frac{1}{Pr}(1+\frac{4}{3}Rd)\varphi''+Nb\theta'\varphi'+Nt(\theta')^2-\frac{c_1\eta}{2a}\theta'+f\theta'\\ &\quad +\frac{1}{Pr}Ec(f'')^2+Ha(f')^2+\lambda_1\theta+Du\varphi''=0\end{aligned} \tag{9}$$

$$\begin{aligned}&\frac{1}{le}\varphi''+\varphi'f-\frac{c_1\eta}{2}\varphi'+\frac{Nt}{Nb}\theta''\\ &\quad -\xi(1+n^*\theta_w\theta)\exp(\frac{-E}{1+\theta_w\theta})\varphi=0\end{aligned} \tag{10}$$

$$X_1''+Lb(f-\frac{A}{2}\eta)X_1'-pe(X_1'\varphi'+(X_1+\Omega)\varphi'')=0 \tag{11}$$

Satisfying the conditions (Eq. 12):

$$\begin{aligned}&f'(0)=1,\ f(0)=f_w,\ \varphi(0)=1,\ \theta(0)=1,\ X_1(0)=1\\ &f'(\infty)=0,\ \varphi(\infty)=0,\ \theta(\infty)=0,\ X_1(\infty)=1\end{aligned} \tag{12}$$

where,

$$\begin{aligned}&\Omega=\frac{\eta_\infty}{\eta_w-\eta_\infty},\ A=\frac{c_1}{a},\ Lb=\frac{\nu}{D_m},\\ &pe=\frac{bW_c}{D_m}(C_w-C_\infty)(1-c_1t),\ le=\frac{\nu}{D_B},\ \xi=\frac{k_r^2}{a},\\ &E=\frac{E_a}{kT},\ \theta_w=\frac{T_w+T_\infty}{T_\infty},\ Pr=\frac{\alpha}{\nu},\ Rd=\frac{4\sigma^*T_\infty^3}{3K^*},\\ &Nb=\frac{\lambda}{\nu}(C_w-C_\infty),\ Nt=\frac{\lambda D_T}{\nu T_\infty}(T_w-T_\infty),\\ &Ec=\frac{\mu a^2x^2}{(T_w-T_\omega)(1-c_1t)^2},\ Ha=\frac{\alpha\sigma B_0^2ax^2}{k(T_w-T_\omega)},\\ &\lambda_1=\frac{Q_0(1-c_1t)}{a(\rho c)_f},\ Du=\frac{D_mk_r}{c_sc_p}(\frac{C_w-C_\infty}{T_w-T_\infty}),\ A=\frac{c_1}{a},\\ &F_n=\frac{k'x}{\sqrt{k}},\ Ha=\frac{(1-c_1t)\sigma B_0^2}{\rho_f a},\ P=\frac{\nu(1-c_1t)}{ka},\\ &Gr=\frac{(1-c_1t)^2(1-C_\infty)(T_w-T_\infty)\beta_g}{a^2x},\\ &Nr=\frac{(\rho_p-\rho_f)(C_w-C_\infty)\varphi g}{(1-C_\infty)\rho_f(T_w-T_\infty)\beta_g},\\ &Rb=\frac{(n_w-n_\infty)(\rho_m-\rho_f)X_1g_{\gamma^*}}{(1-C_\infty)\rho_f(T_w-T_\infty)\beta_g}\end{aligned}$$

where, Le = Lewis number, Ω = Microorganisms concentration difference, ξ = Chemical reaction term, Nt = Brownian motion parameter, θ_w = Relative temperature, Nb = Thermophoresis parameter, E = Activation energy, Rd = Thermal radiation, Ha = Hartman number, Pr = Prandtl number, Ec = Eckert number, λ_1 = Heat Generation, Du = Dufour, Gr = Grashof number, A = Unsteady parameter, Nr = Radiation parameter, F_n = Forcheimmer, and Rb = Rayleigh number.

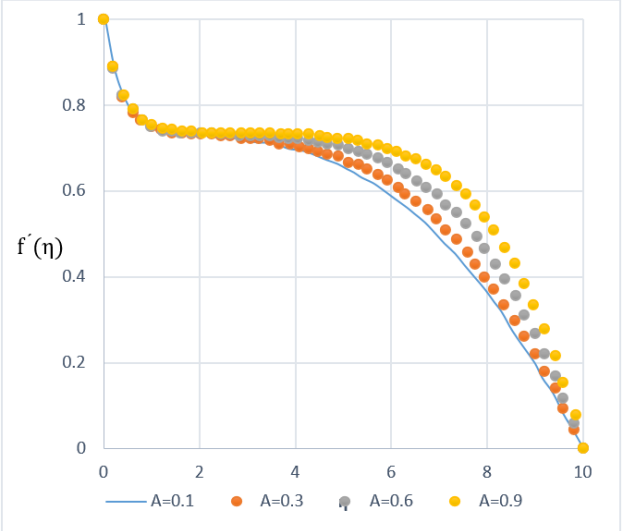

Figure 2. Impact of unsteadiness parameter on the profile of velocity distribution.

The set of non-linear ODEs (8)-(11) with boundary conditions in equation (10) was resolved numerically by the scheme of Runge–Kutta integration with the shooting method of modified Newton–Raphson and with prescribed parameters such as λ, A, P, Ha, Nr, Gr, Rb, Rd, Nb, Pr, Ec, and Nt. The calculations were conducted using a program that utilizes a MAPLE computational and symbolic computer language [24]. The step size $\Delta\eta = 0.001$ was chosen for a convergence measure 10^{-7} to be satisfactory in almost cases. The value of each iteration loop was found with the assignment statement $\eta_\infty = \eta_\infty + \Delta\eta$. The highest amount of parameters λ, A, P, Ha, Nr, Gr, Rb, Rd, Nb, Pr, Ec, and Nt as well as η_∞ is specified as the unidentified boundary conditions values that are not altered at $\eta = 0$ to a prosperous loop with an error of less than 10^{-9}.

3. Results and discussion

3.1 Velocity

Fig. 2 shows the unsteadiness parameter effect on the velocity profile. It can be observed that the profile of the velocity distribution rises with the increasing unsteadiness parameter. The impact of the porous medium permeability (λ) on the profile of velocity is illustrated in Fig. 3. It can be observed that the drag force declines with increasing the porous medium permeability. Due to this, the fluid velocity profile becomes steeper. We can see that as the Hartmann number changes in Fig. 4. In other words, the velocity profile is grown by an increase in the Hartmann number. It can be seen that the profile of velocity is enhanced in the boundary region with an increase in the porosity as shown in Fig. 5. Fluids get more space for flowing and thus their velocity rises. Fig. 6 illustrates that increasing the Grash of (Gr)

parameter causes a decline in the profile of velocity near the plate. It should be noted that as the distance from the screen increases, the speed profile decreases. Fig. 7 shows the buoyancy parameter impact on the profile of velocity. Based on the above results, it can be found that the velocity of fluid decreases when the buoyancy parameter is enhanced. The physical features such as bioconvection Rayleigh number include the buoyancy ratio (resistive) forces, which are responsible for resisting the movement of fluid particles in the entire flow domain. Physically, the effects of buoyancy forces were intensified upon increasing the values of *Rb*, leading to the fluid velocity decline.

3.2 Temperature

Fig. 8 shows the unsteadiness parameter influences on the profile of temperature. It can be observed that the energy distribution profile increases when the unsteadiness parameter increases. According to Fig. 9, the profile of energy distribution is enhanced with the change in Hartmann number. Hartmann number effect generates extra heat, which causes escalations in the fluid temperature. Fig. 10 displays that the energy distribution profile declines near the boundary region with increasing the porosity parameter. According to Fig. 11, the profile of temperature enhances with increasing the Grashof number due to an increase of buoyancy forces and a decrease of viscous forces. Fig. 12 shows the buoyancy parameter impact on temperature. Based on the obtained results, it can be seen that increasing the buoyancy parameter increases the fluid TBL. Fig. 13 shows the bioconvective Rayleigh number effect on the profile of energy. It can be observed that the profile of energy distribution is enhanced by changing the bioconvective Rayleigh number, which can attributed to an increase in the Rayleigh number leading to the resistance of the fluid to the movement and as a result the temperature increases. Fig. 14 shows that when increasing radiation parameter values decrease, the TBL has a decreasing effect on temperature because the growth of the radiation parameter releases thermal energy in the fluid. Fig. 15 displays that the temperature distribu-

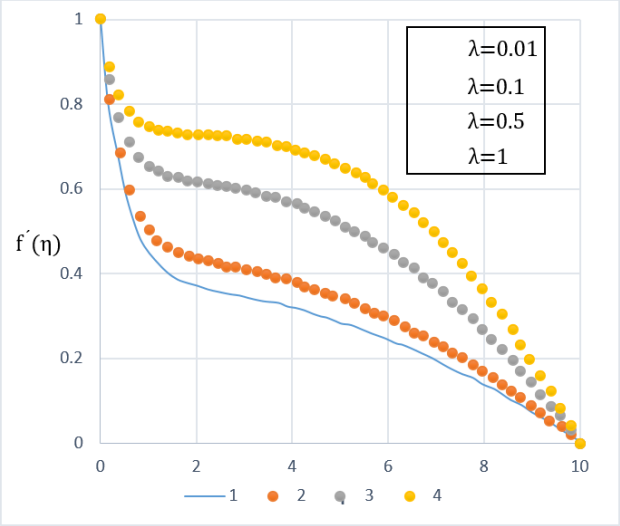

Figure 3. Porous medium inertia parameter's impacts on the profile of velocity distribution.

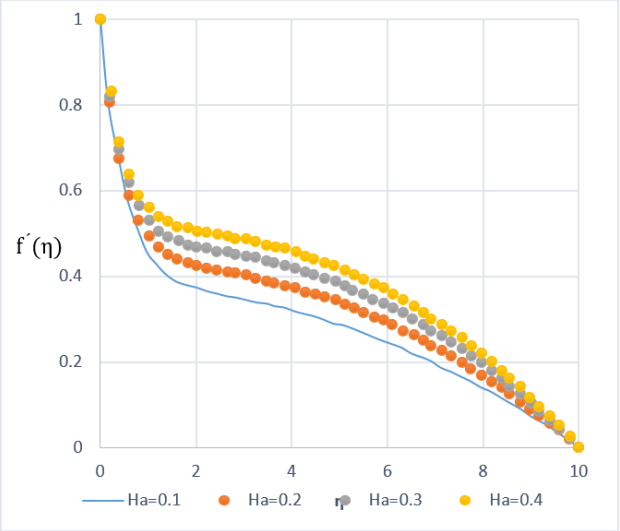

Figure 4. Hartmann number impacts on the profile of velocity distribution.

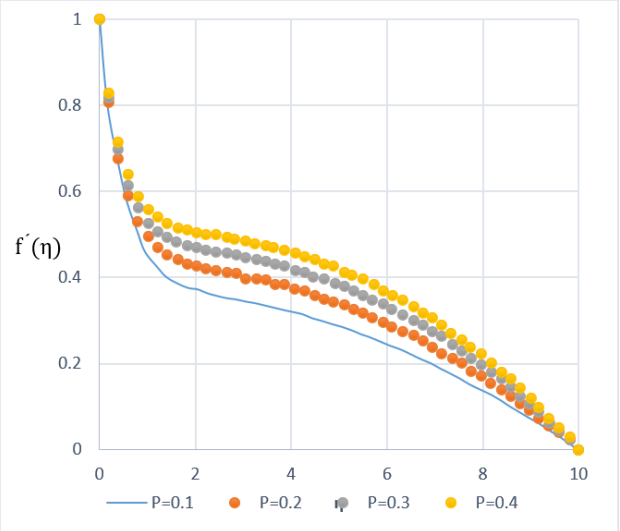

Figure 5. Porosity parameter impacts on the profile of velocity distribution.

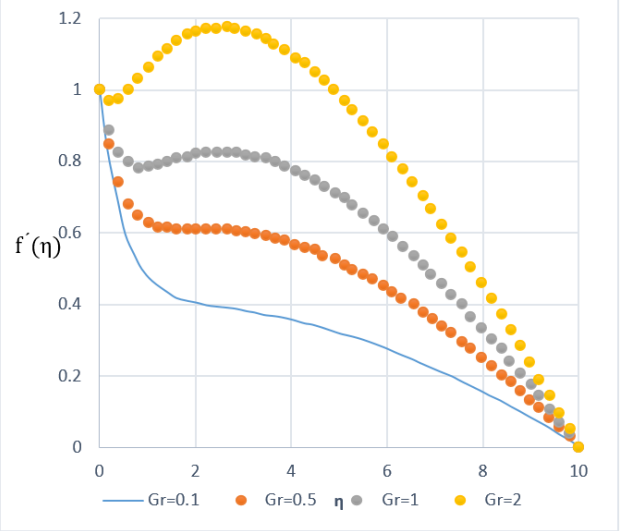

Figure 6. Grashof number impacts on the profile of velocity distribution.

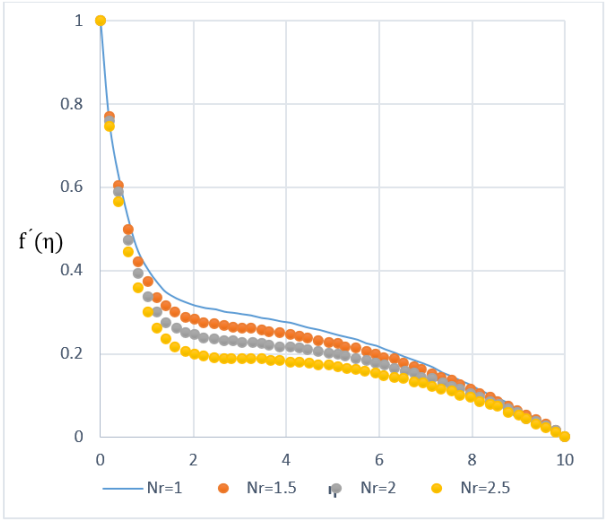

Figure 7. Buoyancy ratio impacts on the profile of velocity distribution.

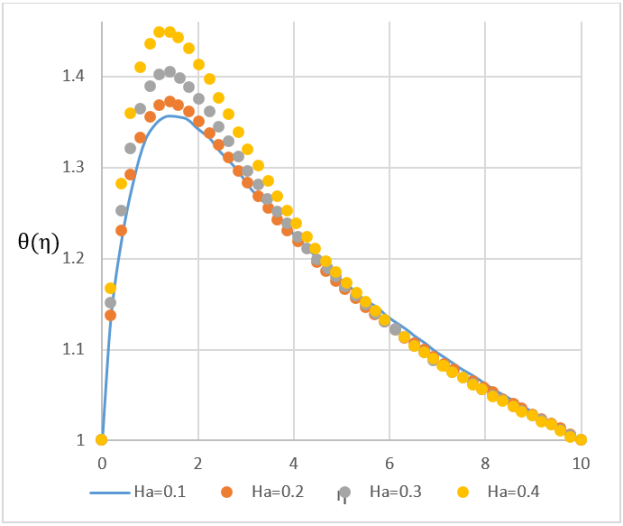

Figure 9. Effects of Hartmann number on the profile of energy distribution.

tion is a growing function of the Prandtl number because the fluid thermal diffusivity rises due to a higher Prandtl number value, which causes to decrease in the thickness of the TBL. Fig. 16 also shows that raising the Eckert number converts the kinetic energy into internal energy using the work performed against the stresses of viscous fluid. Also, the Eckert number reduces the specific heat capacity and heat driving force, which becomes the reason for temperature enhancement. For this reason, increasing the Eckert number (Ec) increases the fluid temperature. In Fig. 17, we apperceived that increasing the internal heat generation (λ) increases the energy distribution profile. Similarly, the heat generation effect produces extra heat, which results in escalations in the fluid temperature.

3.3 Concentration

In Fig. 18, it can be seen that as the unsteadiness parameter (A) increases, the concentration profile of the nanoparticle declines. The effect of an unsteadiness parameter causes

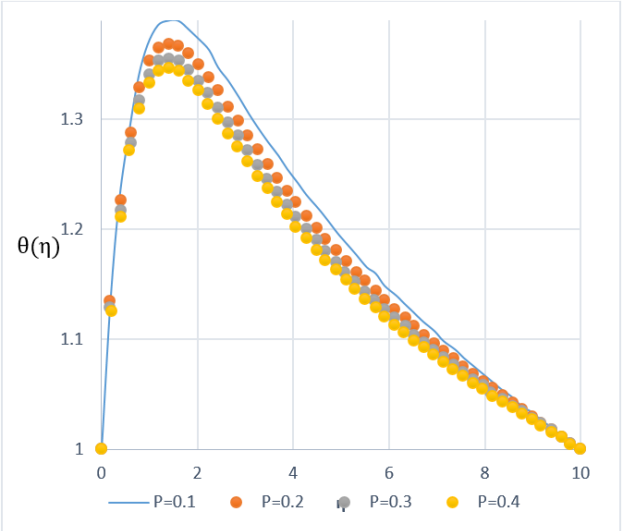

Figure 10. Impacts of Porosity parameter on the profile of energy distribution.

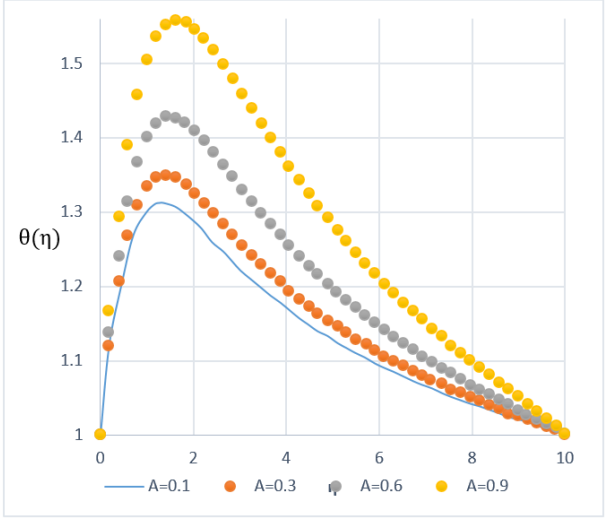

Figure 8. Unsteadiness parameter impacts on the profile of energy distribution.

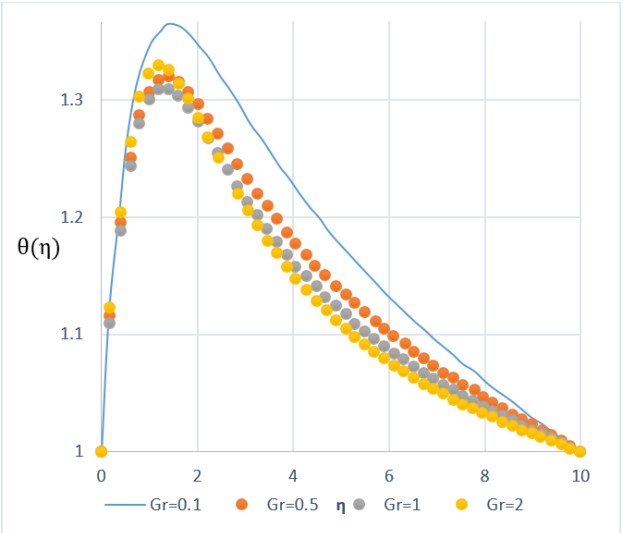

Figure 11. Impacts of Grashof number on the profile of energy distribution.

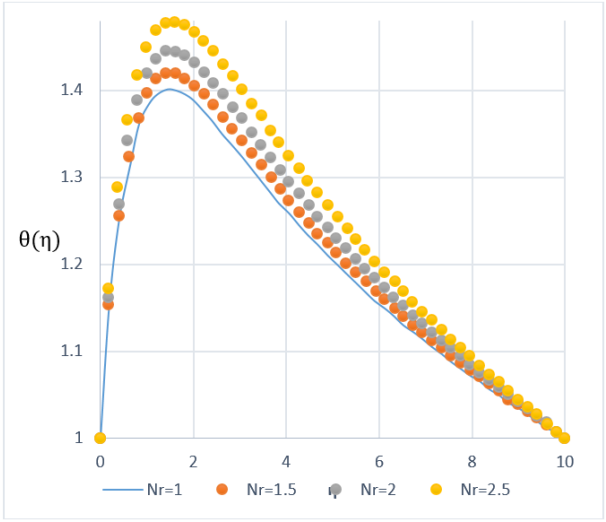

Figure 12. Buoyancy ratio impacts on the profile of energy distribution.

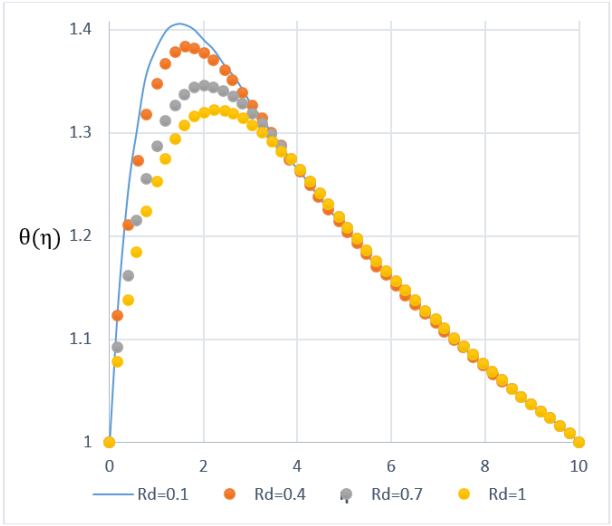

Figure 14. Radiation parameter impacts on the profile of energy distribution.

to increase in boundary layer thickness. Fig. 19 shows that increasing the internal heat generation (λ) increases the concentration profile of nanoparticles. Fig. 20 displays that the concentration profile of nanoparticles reduces with increasing the Hartmann number (Ha). Hartmann number is the ratio of electromagnetic force to viscous force, therefore the thickness of the boundary layer reduces as the Hartmann number increases. In other words, a magnetic effect occurs as the Hartmann number increases, where the Lorentz force is created through the magnetic force and acts against the fluid motion [45]. It indicates that the transverse magnetic field and the transportation processes act opposite. This happens because there is more insistence on the transport mechanisms due to the Lorentz force, and the response is produced by the magnetic impact. Fig. 21 also shows that increasing the buoyancy ratio (Nr) decreases the fluid concentration along the surface. It should be noted that the stronger buoyancy force reduced the fluid flow due to the stretching surface in the downwind direction and thinner

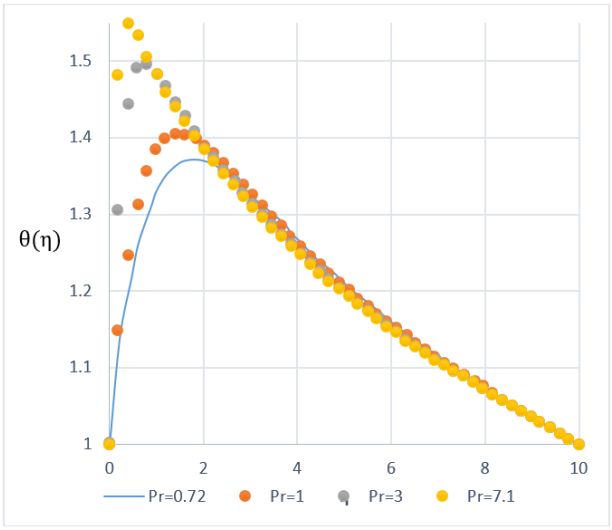

Figure 15. Prandtl number impacts on the profile of energy distribution.

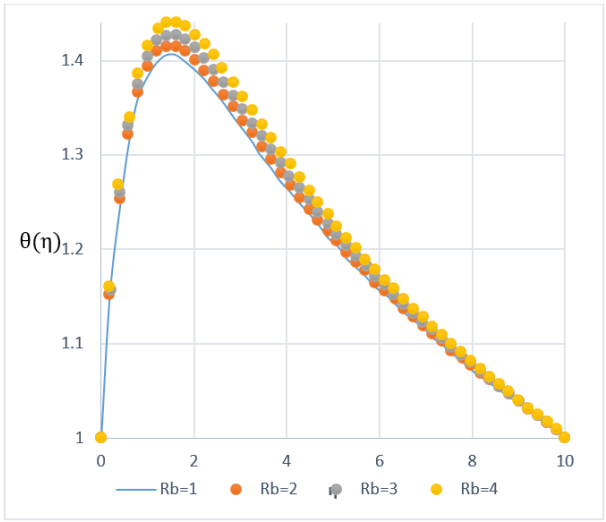

Figure 13. Bioconvective Rayleigh number impacts on the profile of energy distribution.

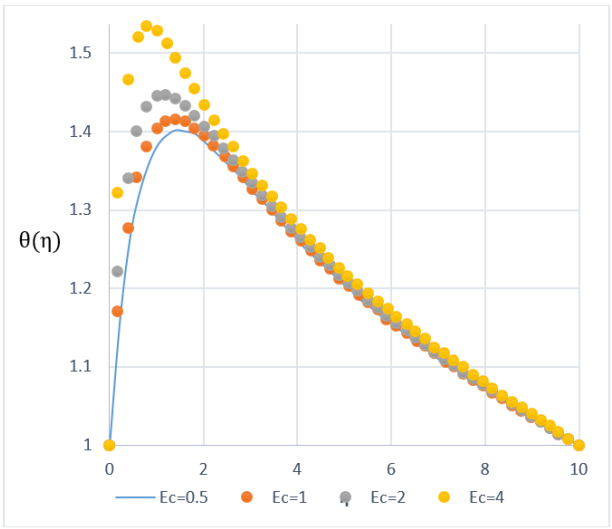

Figure 16. Eckert number impacts on the profile of energy distribution.

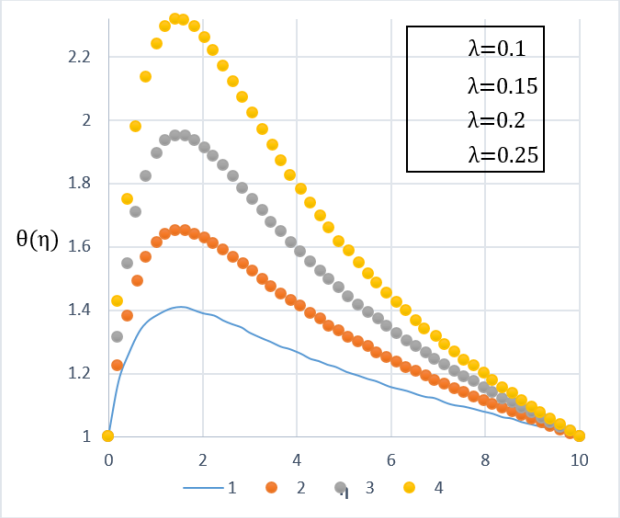

Figure 17. Eckert number impacts on the profile of energy distribution.

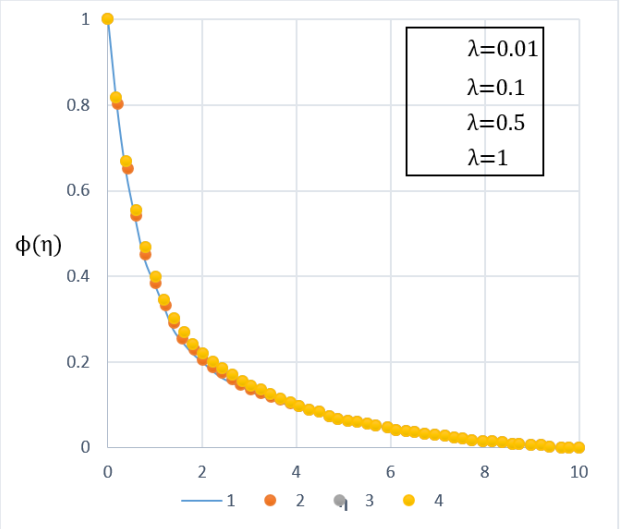

Figure 19. Impacts of internal heat generation (λ) on the profile of nanoparticle concentration.

boundary layer thickness. In Fig. 22, it can be observed that increasing the Radiation parameter (*Rd*) increases the concentration, which is attributed to the increasing concentration boundary layer thickness. Based on Fig. 23, we apperceived that increasing the Prandtl number increases the profile of concentration due to enhancing boundary layer thickness. Fig. 24 shows that the Brownian parameter has a significant effect on the concentration of dimensionless nanoparticles in the fluid. By increasing the Brownian motion parameter, the concentration boundary layer increases, and as a result, enhances the fluid concentration profile. In Fig. 25, a decrease in the concentration profile is observed with the growth of the thermophoresis parameter (*Nb*), which intensifies the concentration profile. It's clear that the thickness of the boundary layer for mass friction function decreases as *Nb* increases, therefore the concentration profile decreases. Fig. 26 shows that enhancing the Eckert number results in a decline in the profile of the nanoparticle concentration. The Eckert number relates the kinetic energy in the flow to enthalpy. As the Eckert number increases, the concentration profile decreases due to internal particle friction converting mechanical energy into thermal energy and also decreases the concentration boundary layer.

4. Conclusion

In this research, bioconvective unsteady Darcy-Forchheimer NF flows with the activation energy and chemical reaction of Arrhenius on a permeable tensile surface were studied. The PDEs of the governing boundary layer were converted as an ordinary differential equation system via a similarity transformation. For different selections of dimensionless parameters of the model, the resultant ODEs were numerically resolved using the Runge–Kutta integration with the shooting method of modified Newton–Raphson. The obtained results are as follows:

1. The unsteadiness parameter, porous medium perme-

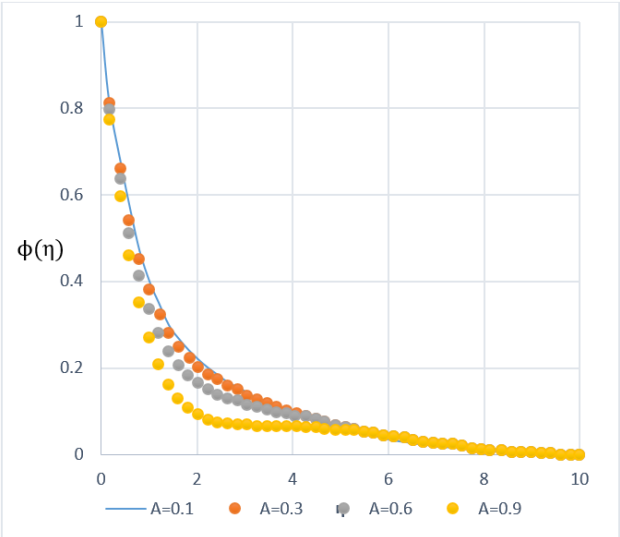

Figure 18. Unsteadiness parameter effects on the profile of nanoparticle concentration.

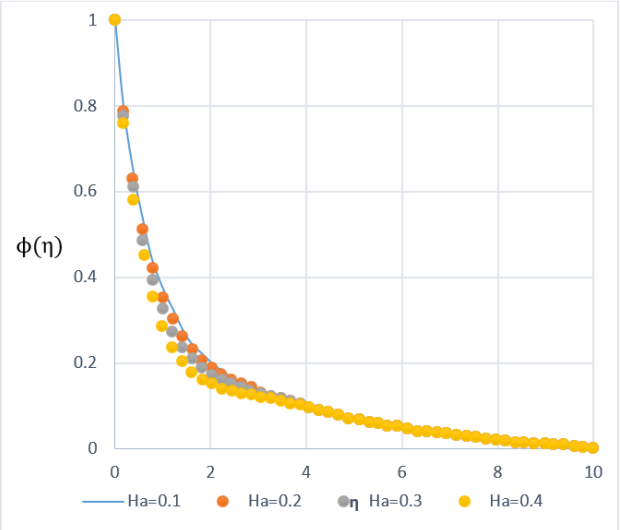

Figure 20. Hartmann number impacts on the profile of nanoparticle concentration.

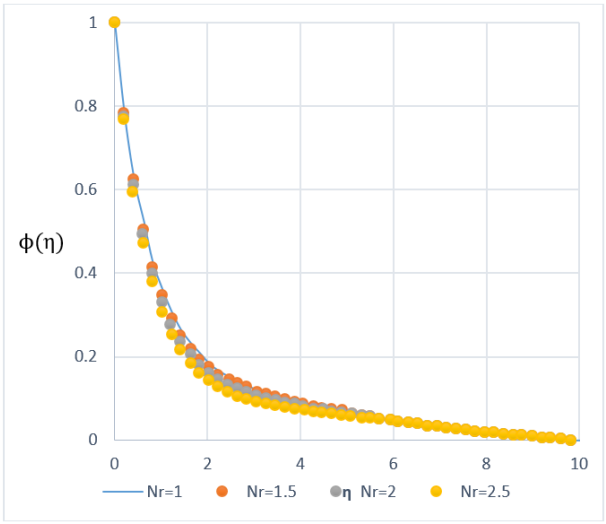

Figure 21. Buoyancy ratio impacts on the profile of nanoparticle concentration.

ability, Hartmann number, porosity parameter, and Grashof parameter increased the velocity profile, while the buoyancy ratio decreased it.

2. Unsteadiness parameter, Hartmann number, buoyancy ratio, bioconvective Rayleigh number, Prandtl number, Eckert number, and internal heat generation raised the temperature profile.
3. The porosity parameter, Grashof number, and radiation parameter led to a decrease in temperature profile.
4. The unsteadiness parameter, Hartmann number, buoyancy ratio, thermophoresis, Prandtl number, and Eckert number reduced the concentration profile.
5. The growth of the parameter of internal heat generation had almost no effect on the concentration profile.
6. The radiation parameter and Brownian motion enhanced the concentration profile.

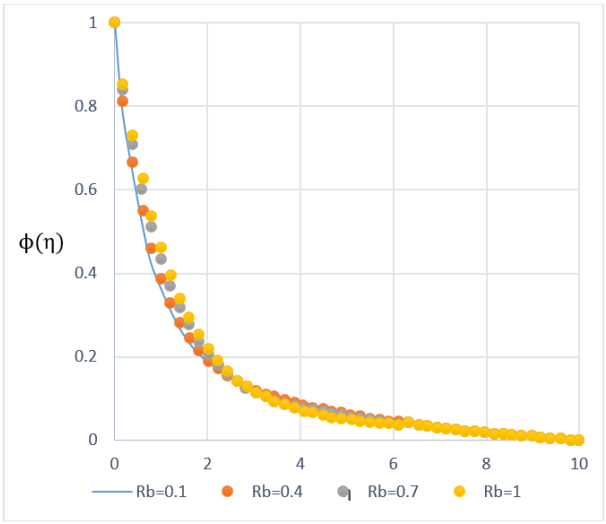

Figure 22. Radiation parameter impacts on the profile of nanoparticle concentration.

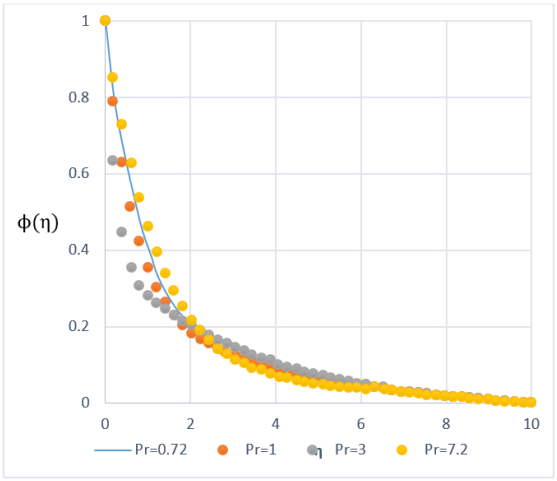

Figure 23. Prandtl number impacts on the profile of nanoparticle concentration.

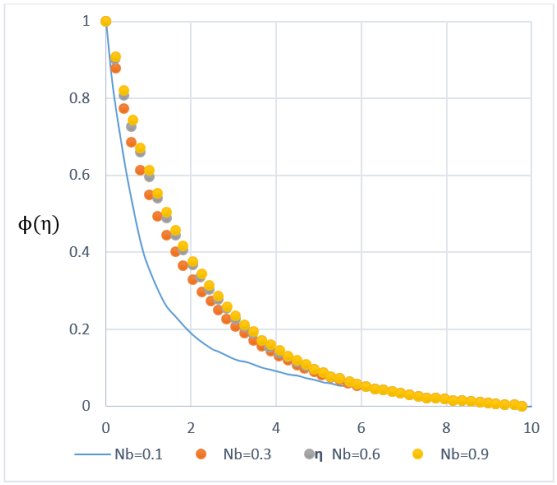

Figure 24. Impacts of Brownian motion on the profile of nanoparticle concentration.

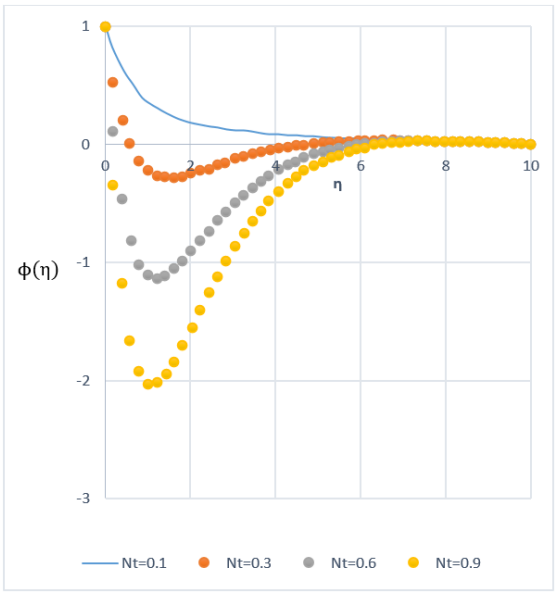

Figure 25. Impacts of thermophoresis on the profile of nanoparticle concentration.

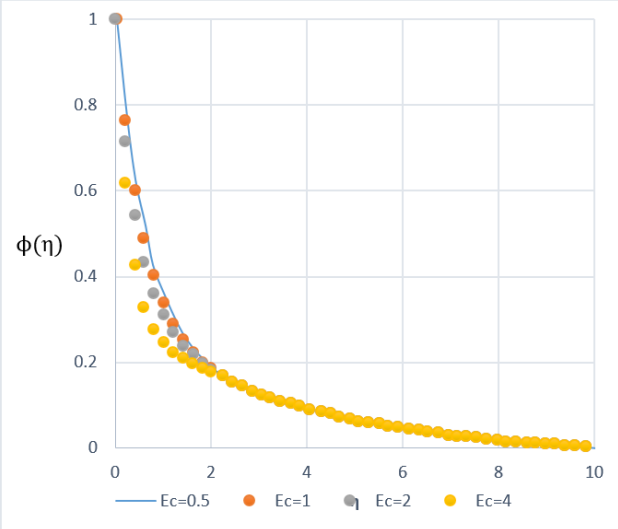

Figure 26. Eckert number impacts on the profile of nanoparticle concentration.

Availability of data and materials
The authors declare that the data supporting the findings of this study are available within the paper.

Conflict of interests
The authors assert that they do not have any identifiable conflicting financial interests or personal relationships that might be perceived to influence the work presented in this paper.

References

[1] R. E. Goldstein. "Green algae as model organisms for biological fluid dynamics.". *Annual Review of Fluid Mechanics*, 47:343–375, 2015.
DOI: https://doi.org/10.1146/annurev-fluid-010313-141426.

[2] E. L. Cussler. "Bioconvection.". *Annual Review of Fluid Mechanics*, 41:87–110, 2009. URL https://journals.scholarsportal.info/browse/00664189.

[3] J. Patten. "Bioconvection: A new approach to drug delivery.". *Trends in Biotechnology*, 34(11):878–887, 2016.

[4] M. Friedrichs and M. Holzner. "Pattern formation in bioconvection triggered by the gradient of light.". *Experiments in Fluids*, 47(5): 753–761, 2009.
DOI: https://doi.org/10.1007/978-1-0716-0421-2_214.

[5] J. Elgeti and G. Gompper. "Emergence of metachronal waves in cilia arrays.". *Proceedings of the National Academy of Sciences*, 110(12): 4470–4475, 2013.
DOI: https://doi.org/10.1073/pnas.1218869110.

[6] L. Zhang and P. Wang. "Enhanced biofuel production through bioconvection.". *Bioresource Technology*, 218:581–588, 2016.
DOI: https://doi.org/10.1016/j.wasman.2007.10.009.

[7] A. Shafiq and T. N. Sindhu. "Statistical study of hydromagnetic boundary layer flow of Williamson fluid regarding a radiative surface.". *Results in Physics*, 7:3059–3067, 2017.
DOI: https://doi.org/10.1016/j.rinp.2017.07.077.

[8] U. S. Choi. "Enhancing thermal conductivity of fluids with nanoparticles.". *Developments and Applications of Non-Newtonian Flows*, 231:99–105, 1995. URL https://www.researchgate.net/publication/236353373_Enhancing_thermal_conductivity_of_fluids_with_nanoparticles.

[9] A. Shafiq, T. N. Sindhu, and Q. M. Al-Mdallal. "A sensitivity study on carbon nanotubes significance in Darcy-Forchheimer flow towards a rotating disk by response surface methodology.". *Scientific Reports*, 11:8812, 2021.
DOI: https://doi.org/10.1038/s41598-021-87956-8.

[10] A. Shafiq, A. B. Çolak, and T. N. Sindhu. "Construction of neural network based intelligent computing for treatment of Darcy-Forchheimer sisko nanofluid flow with Rosseland's radiative process.". *Heat Transfer Research*, 54(9):77–98, 2023.
DOI: https://doi.org/10.1615/HeatTransRes.2023046617.

[11] A. Shafiq, A. B. Çolak, and T. N. Sindhu. "Comparative analysis to study the Darcy-Forchheimer Tangent hyperbolic flow towards cylindrical surface using artificial neural network: An application to Parabolic Trough Solar Collector.". *Mathematics and Computers in Simulation*, 216:213–230, 2023.
DOI: https://doi.org/10.1016/j.matcom.2023.09.014.

[12] A. Shafiq, A. B. Çolak, T. N. Sindhu, and T. Muhammad. "Optimization of Darcy-Forchheimer squeezing flow in nonlinear stratified fluid under convective conditions with artificial neural network.". *Heat Transfer Research*, 53(3):67–89, 2022.
DOI: https://doi.org/10.1615/HeatTransRes.2021041018.

[13] A. B. Çolak, A. Shafiq, and T. N. Sindhu. "Modeling of Darcy-Forchheimer bioconvective Powell Eyring nanofluid with artificial neural network.". *Chinese Journal of Physics*, 77:2435–2453, 2022.
DOI: https://doi.org/10.1016/j.cjph.2022.04.004.

[14] A. Shafiq, A. B. Çolak, and T. N. Sindhu. "Optimization of the numerical treatment of the Darcy-Forchheimer flow of Ree-Eyring fluid with chemical reaction by using artificial neural networks.". *International Journal for Numerical Methods in Fluids*, 95(9):176–192, 2023.
DOI: https://doi.org/10.1002/fld.5147.

[15] A. Shafiq, A. B. Çolak, and T. N. Sindhu. "Modeling of Darcy-Forchheimer magnetohydrodynamic Williamson nanofluid flow towards nonlinear radiative stretching surface using artificial neural network.". *International Journal for Numerical Methods in Fluids*, 95(9):1502–1520, 2023.
DOI: https://doi.org/10.1002/fld.5216.

[16] A. Shafiq, A. B. Çolak, and T. N. Sindhu. "Designing an artificial neural network of nanoparticle diameter and solid-fluid interfacial layer on single-walled carbon nanotubes/ethylene glycol nanofluid flow on thin slendering needles.". *International Journal for Numerical Methods in Fluids*, 93(12):3384–3404, 2021.
DOI: https://doi.org/10.1002/fld.5038.

[17] A. Shafiq, A. B. Çolak, and T. N. Sindhu. "Modeling of Soret and Dufour's convective heat transfer in nanofluid flow through a moving needle with artificial neural network.". *Arabian Journal for Science and Engineering*, 48:2807–2820, 2023.
DOI: https://doi.org/10.1007/s13369-022-06945-9.

[18] M. Jawad, F. Mebarek-Oudina, H. Vaidya, and P. Prashar. "Influence of bioconvection and thermal radiation on MHD Williamson non-Casson fluid flow with the swimming of gyrotactic microorganisms due to porous stretching sheet.". *Journal of Nanofluids*, 11(4):500–509, 2022.
DOI: https://doi.org/10.1166/jon.2022.1863.

[19] B. K. Sharma and R. Gandhi. "Combined effects of joule heating and non-uniform heat source/sink on unsteady MHD mixed convective flow over a vertical stretching surface embedded in a darcy-forchheimer porous medium.". *Propulsion and Power Research*, 11 (2):276–292, 2022.
DOI: https://doi.org/10.1016/j.jppr.2022.06.001.

[20] A. Shafiq, S. A. Lone, T. N. Sindhu, and K. Nonlaopon. "Statistical modelling for the Darcy-Forchheimer flow of Casson cobalt ferrite-water/ethylene glycol nanofluid under nonlinear radiation.". *Symmetry*, 14(8):1717, 2022.
DOI: https://doi.org/10.3390/sym14081717.

[21] A. Shafiq, F. Mebarek-Oudina, T. N. Sindhu, and G. Rasool. "Sensitivity analysis for Walters-B nanoliquid flow over a radiative Riga surface by RSM.". *Scientia Iranica*, 29(3):1236–1249, 2022.
DOI: https://doi.org/10.24200/sci.2021.58293.5662.

[22] F. B. Tadesse, O. D. Makinde, and L. G. Enyadene. "Hydromagnetic stagnation point flow of a magnetic ferrofluid past a convectively heated permeable stretching/shrinking sheet in a darcy-forchheimer porous medium.". *International Research Journal of Pharmacy*, 7: 107–115, 2021.
DOI: https://doi.org/10.1007/s12046-021-01643-y.

[23] N. Vedavathi, G. Dharmaiah, K. Venkatadri, and S. A. Gaffar. "Numerical study of radiative non-Darcy nanofluid flow over a stretching sheet with convective Nield conditions and energy activation.". *Nonlinear Engineering*, 10(1):159–176, 2021.
DOI: https://doi.org/10.1515/nleng-2021-0012.

[24] A. Shafiq, A. B. Çolak, and T. N. Sindhu. "Analyzing activation energy and binary chemical reaction effects with artificial intelligence approach in axisymmetric flow of third grade nanofluid subject to Soret and Dufour effects.". *Heat Transfer Research*, 54(3):75–94, 2023.
DOI: https://doi.org/10.1615/HeatTransRes.2022045008.

[25] L. Zhang, M. M. Bhatti, A. Shahid, R. Ellahi, O. A. Bég, and S. M. Sait. "Nonlinear nanofluid fluid flow under the consequences of Lorentz forces and Arrhenius kinetics through a permeable surface: A robust spectral approach.". *Journal of the Taiwan Institute of Chemical Engineers*, 124:98–105, 2021.
DOI: https://doi.org/10.1016/j.jtice.2021.06.049.

[26] A. Khan, A. Saeed, A. Tassaddiq, T. Gul, S. Mukhtar, P. Kumam, and W. Kumam. "Bio-convective micropolar nanofluid flow over thin moving needle comprising gyrostatic microorganisms.". *Case Studies in Thermal Engineering*, 25:100989, 2021.
DOI: https://doi.org/10.1016/j.csite.2021.100989.

[27] A. Shafiq, T. N. Sindhu, and C. M. Khalique. "Numerical investigation and sensitivity analysis on bioconvective tangent hyperbolic nanofluid flow towards stretching surface by response surface methodology.". *Alexandria Engineering Journal*, 59(6):4533–4548, 2020.
DOI: https://doi.org/10.1016/j.aej.2020.08.007.

[28] M. M. Bhatti, K. Al-Khaled, S. U. Khan, W. Chammam, and M. Awais. "Darcy-Forchheimer higher-order slip flow of Eyring-Powell nanofluid with nonlinear thermal radiation and bioconvection phenomenon.". *Journal of Dispersion Science and Technology*, 44 (2):225–235, 2023.
DOI: https://doi.org/10.1080/01932691.2021.1942035.

[29] U. Habib, S. Abdal, I. Siddique, and R. Ali. "A comparative study on micropolar, Williamson, Maxwell nanofluids flow due to a stretching surface in the presence of bioconvection, double diffusion and activation energy.". *International Communications in Heat and Mass Transfer*, 127:105551, 2021.
DOI: https://doi.org/10.1016/j.icheatmasstransfer.2021.105551.

[30] M. Rahman, F. Haq, P. C. Darab, M. Sallah, S. A. Abdelmohsen, B. M. Fadhl, and B. M. Makhdoum. "Mixed convection and activation energy impacts on MHD bioconvective nanofluid flow with irreversibility assessment.". *Heliyon*, 9(6), 2023.
DOI: https://doi.org/10.1016/j.heliyon.2023.e16490.

[31] M. Jawad, A. Saeed, T. Gul, and A. Bariq. "MHD Darcy-Forchheimer flow of Casson nanofluid due to a rotating disk with thermal radiation and Arrhenius activation energy.". *Journal of Physics Communications*, 5(2):025008, 2021.
DOI: https://doi.org/10.1088/2399-6528/abe4e0.

[32] B. M. Tamilzharasan, S. Karthikeyan, M. K. Kaabar, M. Yavuz, and F. Özköse. "Magneto mixed convection of Williamson nanofluid flow through a double stratified porous medium in attendance of activation energy.". *Mathematical and Computational Applications*, 27(3):46, 2022.
DOI: https://doi.org/10.3390/mca27030046.

[33] S. Rashid, M. I. Khan, T. Hayat, M. Ayub, and A. Alsaedi. "Darcy-Forchheimer flow of Maxwell fluid with activation energy and thermal radiation over an exponential surface.". *Applied Nanoscience*, 10:2965–2975, 2020.
DOI: https://doi.org/10.1007/s13204-019-01008-2.

[34] A. Shafiq, G. Rasool, and C. M. Khalique. "Significance of thermal slip and convective boundary conditions in three-dimensional rotating Darcy-Forchheimer nanofluid flow.". *Symmetry*, 12(5):741, 2020.
DOI: https://doi.org/10.3390/sym12050741.

[35] T. Hayat, A. Aziz, T. Muhammad, and A. Alsaedi. "Darcy-Forchheimer three-dimensional flow of Williamson nanofluid over a convectively heated nonlinear stretching surface.". *Communications in Theoretical Physics*, 68(3):387–394, 2017.
DOI: https://doi.org/10.1088/0253-6102/68/3/387.

[36] A. R. Bestman. "Natural convection boundary layer with suction mass transfer in a porous medium.". *International Journal of Energy Research*, 14:389–396, 1990.
DOI: https://doi.org/10.1002/er.4440140403.

[37] A. Dawar, Z. Shah, and S. Islam. "Mathematical modelling and study of MHD flow of Williamson nanofluid over a nonlinear stretching plate with activation energy.". *Heat Transfer*, 50:2558–2570, 2021.
DOI: https://doi.org/10.1002/htj.21992.

[38] F. E. Alsaadi, T. Hayat, M. I. Khan, and F. E. Alsaadi. "Heat transport and entropy optimization in flow of magneto-Williamson nanomaterial with Arrhenius activation energy.". *Computer Methods and Programs in Biomedicine*, 183:105051, 2020.
DOI: https://doi.org/10.1016/j.cmpb.2019.105051.

[39] R. Muhammad, M. I. Khan, M. Jameel, and N. B. Khan. "Fully developed Darcy-Forchheimer mixed convective flow over a curved surface with activation energy and entropy generation.". *Computer Methods and Programs in Biomedicine*, 188:105298, 2020.
DOI: https://doi.org/10.1016/j.cmpb.2019.105298.

[40] S. H. Danook, Q. K. Jasim, and A. M. Hussein. "Nanofluid convective heat transfer enhancement elliptical tube inside circular tube under turbulent flow.". *Mathematical and Computational Applications*, 23(4):78, 2020.
DOI: https://doi.org/10.3390/mca23040078.

[41] W. Jamshed, M. Goodarzi, M. Prakash, K. S. Nisar, M. Zakarya, and A. H. Abdel-Aty. "Evaluating the unsteady Casson nanofluid over a stretching sheet with solar thermal radiation: An optimal case study.". *Case Studies in Thermal Engineering*, 26:101160, 2021.
DOI: https://doi.org/10.1016/j.csite.2021.101160.

[42] M. Alghamdi, A. Wakif, T. Thumma, and U. Khan. "Significance of variability in magnetic field strength and heat source on the radiative-convective motion of sodium alginate-based nanofluid within a Darcy-Brinkman porous structure bounded vertically by an irregular slender surface.". *Case Studies in Thermal Engineering*, 28: 101428, 2021.
DOI: https://doi.org/10.1016/j.csite.2021.101428.

[43] M. B. Arain, M. M. Bhatti, A. Zeeshan, T. Saeed, and A. Hobiny. "Analysis of Arrhenius kinetics on multiphase flow between a pair of rotating circular plates.". *Mathematical Problems in Engineering*, 2020:1–17, 2020.
DOI: https://doi.org/10.1155/2020/2749105.

[44] E. A. Algehyne, E. R. El-Zahar, and S. H. Elhag. "Investigation of thermal performance of Maxwell hybrid nanofluid boundary value problem in vertical porous surface via finite element approach.". *Scientific Reports*, 12:2335, 2022.
DOI: https://doi.org/10.1038/s41598-022-06213-8.

[45] A. Shafiq, F. Mebarek-Oudina, T. N. Sindhu, and A. Abidi. "A study of dual stratification on stagnation point Walters' B nanofluid flow via radiative Riga plate: a statistical approach.". *The European Physical Journal Plus*, 136:407, 2021. DOI: https://doi.org/10.1140/epjp/s13360-021-01394-z.